Highlights of Collaborated Research

Collaborative works with outside researches are carried out in consideration of the joint research program. Accepted applications are performed in following each division and facility of IMR.

1) Research Laboratories

Joint research conducted by out side researchers and IMR staff members at each research laboratory. Three categories; “Research in priority areas”, "General Research" and “Exploratory Research for Young Researchers” are prepared.

2) International Research Center for Nuclear Materials Science

This facility is open to university scientists all over Japan to support experiments using Japan Material Test Reactor, JMTR, the experimental breeder reactor, JOYO and the test reactor, JRR-3 operated by JAEA (Japan Atomic Energy Agency). The overseas reactor, BR2, located at the Belgian Nuclear Research Center, is also used for irradiation experiments. This facility acts as a hub for international collaborations; specimens irradiated in overseas reactors are accepted here for post-irradiation examination by participating university researchers. Research subjects covered here include fundamental studies and R&D on fusion structural materials, high heat-flux materials, and a variety of functional materials, as well as engineering-oriented studies for the safety of light water reactors and basic researches supporting them. Materials studies utilizing radio-isotopes are also being conducted.

3) Advanced Research Center of Metallic Glasses

This center was established in May 1987 as the research center for the development of new advanced materials for the 21st century, reorganized in May 1996 and April 2005. The main purpose of the research in this laboratory is to establish fundamentals and control techniques for synthesizing artificial substances, especially the metallic glasses, and to seek for the possibility of applying them as multi-functional materials for high technology, such as materials for energy saving, materials for environmental and ecology, structural materials, electronic information materials, biomaterials and materials for social welfare, etc.

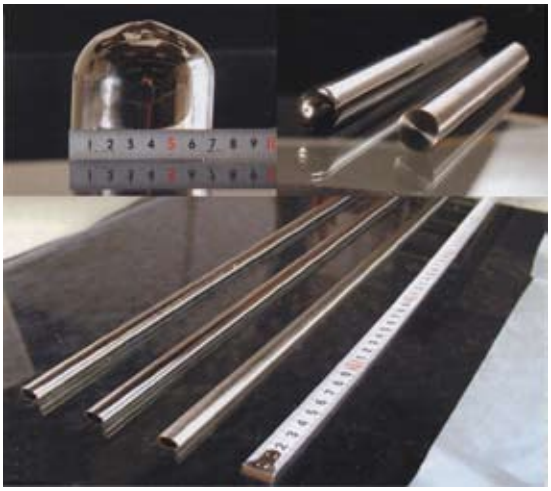

4) High Field Laboratory for Superconducting Materials

This laboratory restarted in 2001, succeeding “High Field Laboratory for Superconducting Materials” which was established in 1981. The main equipment is a hybrid magnet which generates steady high magnetic fields up to 31T. In addition, many cryogen-free superconducting magnets which have been developed by our laboratory are installed. Especially, we succeeded in developing the world’s first cryogen-free hybrid magnet, which generates 27.5 T. The laboratory also provides instruments for measuring various physical properties. These facilities are open to scientists and engineers on superconductors and other materials research.

5) International Frontier Center for Advanced Materials (IFCAM)

The material sciences are fundamentally interdisciplinary and global in nature, involving a variety of academic and engineering fields, in order to achieve better, less-expensive and more eco-friendly functional matter. Clever development and wise use of advanced materials are the foundation of all improved human activity in this new century. Based on the extensive successful research record of IMR, IFCAM was approved and founded in 2002 with a mission to serve as an *international think-tank in materials research.* To foster further international collaboration, liaison offices of IFCAM have been established at Cambridge University, Harvard University, Stanford University, the Swedish Royal Institute of Technology, and the Institute of Physics in China.

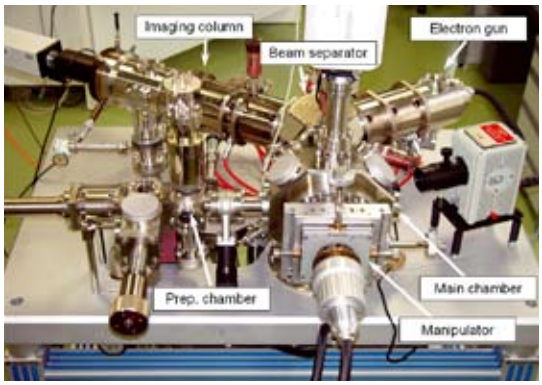

Fig. Low energy electron microscope in IFCAM.

6) Osaka Center for Industrial Materials research

The Osaka Center was established at Osaka as a special unit in IMR in April 2006 based on the agreement between Tohoku University and Osaka Prefecture Government. It is a laboratory dedicated to research and development of nano-structured metallic materials from the application viewpoints based on the basic research in the material science, chemistry and physics associated with research organizations in the Kansai region. Research in the Osaka Center is focused in particular on the understanding of the fundamental properties of nano-structured metallic materials and the rapid realization of their application to industry, in particular, the small and medium enterprises in Osaka area.

7) Center for Computational Materials Science

This center was developed from the Laboratory of Materials Information Science which was established in February 1989. Its main tasks are 1) administration and maintenance of the supercomputing system in this Institute, 2) maintenance of a supercomputing system network, 3) general support for the usage of the supercomputing system, 4) support of materials design by supercomputing simulation with vectorization and parallelization, 5) construction of factual database for materials in nonequilibrium phase , and 6) support of activity of Nanotechnology group on SINET3 and Asian Consortium for Materials Science, ACCMS-VO.

8) International Collaboration Center (ICC-IMR)

This Center was established in April 2008. The mission is to serve as an international center for materials research and to encourage the international collaboration on researches of IMR. The International School on advanced materials, international workshops are coordinated. The Center hosts the foreign visiting scientists who collaborate on research with members of IMR.

Dislocations of ZnO Single Crystal Examined by X-ray Topography and Photoluminescence

Damages induced by indentation in ZnO (0001) wafers were considered to lead to dislocated regions from X-ray topographic images. Photoluminescence intensities of 2.4 eV deep emission band in ZnO decreased drastically, with increasing in annealing temperature up to 800˚C, irrespective of dislocated or nondislocated regions. The development of a new emission band 2.8–3.0 eV was found in non-damaged ZnO through annealing at 700 and 800 ˚C, which suggests that dislocations suppress the development of the new peak.

Wide band-gap oxide-semiconductors have attracted keen attention for optical devices, liquid crystal displays and solar cells. ZnO possesses a direct band-gap of 3.4 eV as well as a large exciton binding energy of 60 meV, which is about three times larger than that of ZnSe and GaN. Thus, ZnO is one of the most promising materials for various kinds of applications in light-emitting devices from blue- to ultraviolet wavelength range, gas sensors, ltrasonic oscillators and acoustic wave transducers. For homo-epitaxial growth of materials for such applications, the necessity of ZnO substrates, of high quality with low dislocation density, is drastically increasing. Such dislocations lead to inhomogeneity of their optical properties as well known in GaN [1]. Dislocations are considered to be rather mobile in ZnO than in GaN and AlN from the difference in their hardness. However, up to now far less has been known on dynamic and optical properties of such dislocations in ZnO except a few papers.

X-ray topography is effective to identify dislocations and their distribution in materials. Indeed, we applied transmission X-ray topography to observe dislocations and succeeded in correlating them to their optical properties in high quality P-doped ZnTe crystals [2]. The density of grown-in dislocations was 7,000 cm^{-2} approximately. By the photo-luminescence (PL) measurement, it was found that the majority of the phosphorus impurities exist in the area where many dislocations are observed in X-ray topographic images, suggesting the probability of impurity accumulation on dislocations during the growth process. The present study was undertaken with the above mentioned on X-ray topographic observation and PL characteristics of dislocations in ZnO crystals.

ZnO single crystals studied in the present work were undoped (n-type, carrier concentration of 3×10^{15} cm^{-3}, resistivity of 30 Ωcm, mobility of 10^2 cm^2/Vs), grown by the hydrothermal method (Scientific Production Company GOODWILL, RUSSIA). The ZnO wafers with (0001) surfaces were in square shape, approximately $10 \times 10 \times 0.5$ mm^3 in size, with sides parallel to [1100] and [11-20]. Density of grown-in dislocations was approximately 500 cm^{-2}. First, by the ZnO wafers were thinned by mechanical polishing and then by chemically polishing in a solution of HCl: H_2O = 1:5 for 60 s at room temperature to X-ray transparency. Each wafer was damaged partly by indentation under 5 N for 5 s with a diamond Knoop with 0.5 mm interval at room temperature in order to introduce dislocated regions. Then, such wafers were cut into two parts for annealing at elevated temperature 500, 600, 700 and 800 ˚C for 5 min under N_2 gas atmosphere (0.1 MPa).

Dislocations of grown-in and indentation-induced in ZnO wafers were observed by means of transmission X-ray topography using Borrmann effect with 11-20 diffraction of Mo $K\alpha_1$ radiation from an X-ray generator

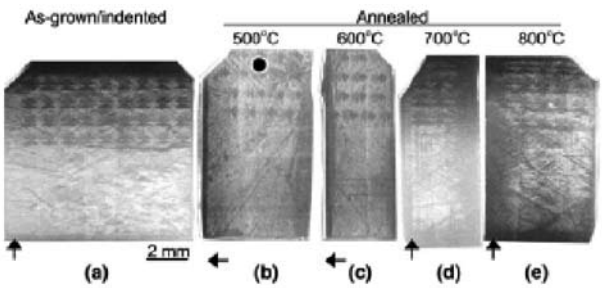

Fig. 1 Transmission x-ray topograph of high quality undoped ZnO single crystal (0001). The *g* vectors are indicated each of the figure.

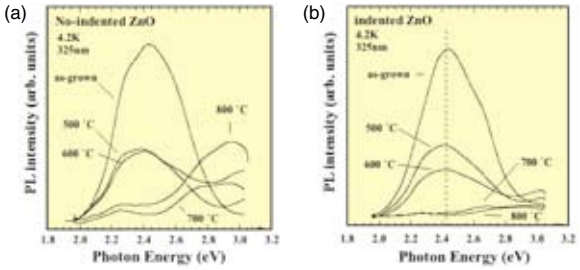

Fig. 2 PL spectra of undoped ZnO single crystal (0001) at 4.2 K in no-indented area (a) and indented area (b).

RIGAKU RU-500. The PL measurement was carried out using a grating monochromator and a photomultiplier at 4.2K. The sample was excited by a 10-mW He-Cd laser, emitting at 325 nm and density of 150 W/cm^2.

Fig. 1 shows transmission X-ray topographic images of high quality undoped ZnO single crystals. The 11-20 diffraction condition is indicated in each figure by *g* vector. Upper part of each wafer was damaged by indentation. In Fig. 1(a) a few dislocations can be seen in the non-indented area of the as-grown ZnO wafer besides some scratches generated during polishing preparation. In the as-grown wafer, images of each indentation are rather sharp and large around the indented center. With increasing temperature of annealing, such images lose their sharpness and become small slightly by annealing at 500 and 600 ˚C. In wafers annealed at 800 ˚C, images are seen to be elongated along <1120> directions from the indented centers. Thus, it is supposed that some dislocations are induced around such indented parts, though detailed observations using transmission electron microscopy should be conducted to clarify how dislocations develop from such indentation during annealing.

Figs. 2(a) and (b) show PL spectra obtained from the no-indented and indented areas, respectively, of ZnO (0001) wafers measured at 4.2 K. Deep emission band around 2.4 eV can be clearly seen in both no-indented and indented areas in the as-grown wafer. The band is known as green band that is related to oxygen vacancy (V_O) [3]. In an increase in annealing temperature, PL intensity of the emission band around 2.4 eV decreases in both no-indented and indented areas. This means that the V_O defects annihilate with increasing annealing temperature. Si multaneously, a new emission band around 2.8–3.0 eV is observed to develop in PL spectra of no-indented area by the annealing at 700 and 800 ˚C. Contrarily, there is observed no such emission band developing around 2.8 eV in indented area. That is, there is no deep emission observed in PL spectra of the indented area annealed at temperatures higher than 700 ˚C. The decrease of 2.4 eV emission band may be annihilation of oxygen vacancies or modification to some complexes promoted at elevated temperatures. Though the origin of the 2.8–3.0 eV emission band is not identified at present, if they relate to radiative recombination defects formed at elevated temperatures, dislocations may suppress their development by absorbing defects relevant to the emission band.

References

[1] I. Yonenaga, H. Makino, S. Itoh, T. Goto, T. Yao, J. Electron. Mater. **35**, 717 (2006).
[2] K. Yoshino, T. Kakeno, M. Yoneta, I. Yonenaga, J. Mater, Sci.: Mater. Electron. **16**, 445 (2005).
[3] M. Yoneta, K. Yoshino, M. Ohishi, M. Honda, H. Saito, Phys. Stat. Sol. (C) **3**, 1185 (2006).

Contact to
Kenji Yoshino (Department Electrical and Electoronic Engineering University of Miyazaki)
e-mail: yoshino@pem.miyazaki-u.ac.jp
Ichiro Yonenaga (Physics of Crystal Defects Division)
e-mail: yonenaga@imr.tohoku.ac.jp

Developments of Optical and Electronic Devices with High Performance Based on Si/Ge Heterostructures

Si-based optical and electronic devices with high performances were developed by Si/Ge heterostructures. Room-temperature resonant luminescence with significantly high efficiency and spectral purity was realized by embedding Ge quantum dots in optical resonators. Extremely high mobilities exceeding current Si devices were also obtained from strained Ge channels grown on SiGe virtual substrates.

Si-based light-emitting devices are highly required for realization of silicon-based optoelectronic integrated circuit. Light emission from Si is inevitably prevented by its indirect band gap nature. In order to overcome this inherent difficulty, Ge quantum dots (QDs) formed on Si have been intensively studied. However, room-temperature light-emission efficiency from Ge QDs-based structures is very low and far from practical applications. Optical resonators are well known to be capable of enhancing the quantum efficiency, where the luminescence in the optical resonator is selectively enhanced by the Purcell effect. In this study, we combined Ge QDs with optical resonators such as photonic crystal microcavity (Fig. 1 (a)), microdisk and microring resonators to modify and enhance the spontaneous emission from Ge QDs.

Fig.1 (b) shows micro-PL spectra obtained from Ge QDs embedded microring resonators. Very sharp resonant peaks are obviously observed in the wavelength range from 1.3 to 1.5 μm while the reference spectrum obtained from unprocessed region reveals no such peak. The sharp peaks were confirmed by numerical simulations to correspond to whispering gallery mode (WGM) and their quality factors were found to be as high as 1800-2200. The quality factor was further enhanced through optimization of the resonator structures up to 3300 which was a surprisingly high value for Si-based light emitting structures. Note that room-temperature photoluminescence with significantly high efficiency and spectral purity was obtained from Ge QDs embedded photonic crystal microcavities and microdisc resonators [1] as well as the microring resonator.

Channel engineering for carrier mobility enhancement has been recognized as essential technology for future CMOS circuits since further scaling is now reaching its limitation. Although the strained-Si

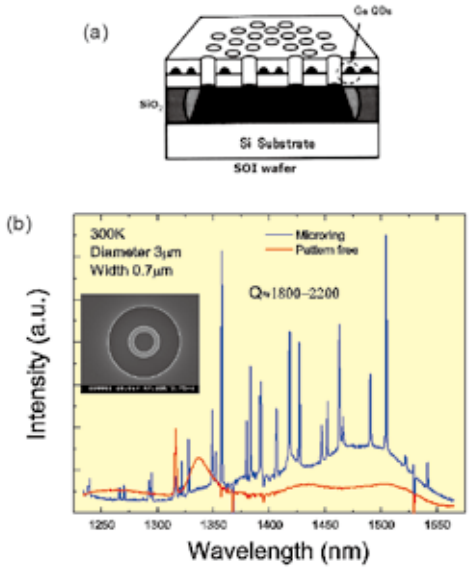

Fig. 1 (a) Schematic of Ge QDs embedded photonic crystal microcavity. (b) PL spectra obtained from microring structure.

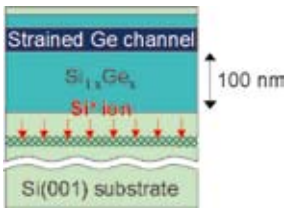

Fig. 2 Strained Ge channel structures on SiGe virtual substrates fabricated by ion implantation technique.

channel has already been involved into mass production, mobility enhancements are still not sufficient particularly for holes. Ge channel is one of the most attractive candidates due to its inherent much higher mobility over strained Si. Moreover, strain introduction is known to further enhance the mobility. Development of strain-induced Ge channel is, therefore, another target of our research project.

The typical structure fabricated here is illustrated in Fig.2. Ion implantation technique was developed to produce high quality thin SiGe virtual substrates which were indispensable for realization of strained-Ge channel devices. This technique was based on intentional introduction of ion-implantation defects into the Si substrates or SiGe virtual substrates. The epitaxial overgrowth was performed on the ion-implanted substrates, leading to effective strain relaxation of the overgrown layer. We obtained considerable relaxation enhancements by the ion implantation with optimum conditions and realized SiGe virtual substrates with one order of magnitude smaller surface roughness (~0.3 nm) and thickness (~100 nm) than conventional virtual substrates.

High quality Ge channels with extremely high compressive strains up to 3% were formed on SiGe virtual substrates by low temperature growth via MBE. Room temperature mobilities higher than 1500 cm^2/Vs were obtained on the developed SiGe virtual substrates with extremely small thickness, which opened the route to practical device applications of strained Ge channels. We also showed the maximum channel mobility exceeds 3000 cm^2/Vs, the highest value ever reported. Moreover, systematic study of magnetotransport properties demonstrated that the hole effective mass can be reduced by increasing the strain [2]. It was also found that the effective mass sensitively changes with hole density modification through gating [3].

In conclusion, both optical and electronic devices were developed based on Si/Ge heterostructures and excellent room-temperature properties were presented, indicating the introduction of Si/Ge is the most promising way for realization of Si-based optoelectronic devices.

References

[1] J. S. Xia, K, Nemoto, Y. Ikegami, N. Usami and Y. Shiraki: Appl. Phys. Lett. **91**, 011104 (2007).
[2] K. Sawano, Y. Kunishi, K. Toyama, T. Okamoto, N. Usami, K. Nakagawa and Y. Shiraki: Physica E **40**, 2122-2124 (2008).
[3] K. Sawano, Y. Kunishi, Y. Satoh, K. Toyama, K. Arimoto, T. Okamoto, N. Usami, K. Nakagawa and Y. Shiraki: Appl. Phys. Express **1**, 011401 (2008).

Contact to
Yasuhiro Shiraki (Musashi Institute of Technology)
e-mail: yshiraki@sc.musashi-tech.ac.jp
Noritaka Usami (Crystal Physics Division)
e-mail: usa@imr.tohoku.ac.jp

Improvement of Biocompatibility of Titanium Implants by Calcium Phosphate Coating Using RF Magnetron Sputtering

An amorphous calcium phosphate film coated on screw-type Ti-6Al-4V implants with a blast-treated surface by using radiofrequency magnetron sputtering was evaluated in vivo. The coated specimens were implanted into the femur of Japanese white rabbits. The removal torque of the implants was statistically improved by coating the amorphous calcium phosphate film two weeks after implantation.

Titanium materials can be directly connected to living remodeling bones at the optical microscopic level, i.e., osseointegration. However, it is known that more than three months are required to obtain a strong fixation between titanium implants and bones and the strength of the fixation might be influenced by the state of bones. Coating calcium phosphate on titanium implants is one of the methods to improve the osseointegration of titanium implants. Amorphous calcium phosphate (ACP) fabricated by radiofrequency (RF) magnetron sputtering is a candidate coating material for titanium implants.

An increase in the percentage of bone-implant contact was demonstrated in titanium cylinders with an ACP coating film by performing animal experiments in which the cylinders were implanted into the mandibles of beagle dogs[1]. This increase in the percentage as compared to that for uncoated titanium cylinders was observed 8–12 weeks after implantation. ACP-coated titanium implants were suggested to effectively exhibit a rapid and strong fixation to bones.

The blast treatment of titanium implants is a common technique to improve the adhesion of the bonding between the titanium implants and bones due to an increase in surface roughness. Therefore, the animal experiments were performed using ACP-coated screw-type Ti-6Al-4V implants with a blast-treated surface. The coated Ti-6Al-4V specimens were implanted into the femur of Japanese white rabbits[2]. The thickness of the ACP coating film was 0.5 μm and the average roughness of the Ti-6Al-4V implants was 4.6 μm. Figure 1 shows the cross section of the ACP film fabricated on the blast-treated Ti-6Al-4V plate. The ACP coating film can be efficiently coated over the entire blast-treated Ti-6Al-4V surface. The surface being rough even after coating is one of the advantages of the RF magnetron sputtering process, which can uniformly fabricate a thin coating film.

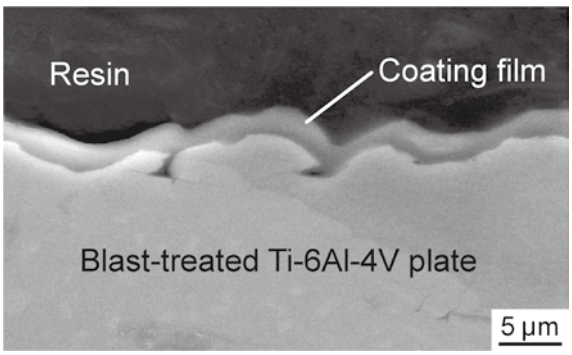

Fig.1 Scanning electron micrograph of cross-section of ACP film coated on blast-treated Ti-6Al-4V plate.

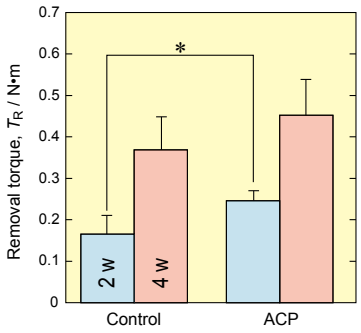

Fig.2 Removal torque of uncoated (control) and ACP-coated screw-type Ti-6Al-4V implants with blast-treated surface from femur of Japanese white rabbits after implantation for two and four weeks. (*$p < 0.05$)

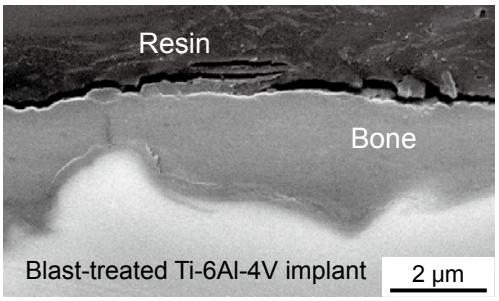

Fig.3 Scanning electron micrograph of cross-section of ACP-coated screw-type Ti-6Al-4V implant with blast-treated surface after removal torque measurement (four week implantation).

Figure 2 shows the removal torque of the coated implants from the femur of a Japanese white rabbit. It increases with the duration of implantation, and as compared to the removal torque of the uncoated titanium implant (control), it is statistically improved by coating the ACP films two weeks after the implantation. The cross-section of the titanium implants coated with the ACP film after removal torque measurements is shown in Fig.3. A smooth and uniform interface is observed between the new bone and the blast-treated implant.

These in vivo studies suggest that the coating of a sputtered ACP film on titanium implants is effective for the rapid and strong fixation of blast-treated titanium implants to bones.

References

[1] K. Ueda, T. Narushima, T. Goto, M. Taira and T. Katsube, Biomed. Mater., **2**, S160 (2007).
[2] T. Narushima, K. Ueda, T. Goto, T. Katsube, H. Kawamura, H. Nakagawa and M. Taira, J. Jpn. Soc. Power and Powder Metall., **55**,318 (2008).

Contact to
Takayuki Narushima (Department of Materials Processing, Tohoku University)
e-mail: narut@material.tohoku.ac.jp
Takashi Goto (Multi-functional Materials Science Division)
e-mail: goto@imr.tohoku.ac.jp

Exchange Coupling and Energy-Level Crossing of 4f-3d Heterometallic Coordination Compounds

We have reported several 4f-3d heterometallic complexes, such as [Dy_2Cu], [Dy_4Cu], and [$(Dy_2Cu_2)_n$], behaving as a single-molecule magnet (SMM). Though several 4f-3d-based SMMs are known to date, the magnitude of exchange coupling has never been determined before our work. We have proposed a plausible mechanism for the quantum tunneling of the magnetization for the above compounds based on the well-defined exchange couplings.

SMM exhibits magnetic hysteresis from the single-molecular origin; namely, slowing down of the rate of magnetization reorientation due to a high energy-barrier. Lanthanide ions seem just suitable for development of SMMs because the barrier is related to strong magnetic anisotropy and large spins. Actually, the above Dy-Cu compounds showed slow magnetization reorientation, as clarified by pulsed-field and ac magnetic measurements [1-3]. Quantum tunneling of magnetization, observable as magnetization jumps in a hysteresis curve, is also characteristic of SMMs. We investigated the exchange couplings and energy-level structures of these compounds. High-frequency (HF)-EPR results on linear [Dy_2Cu] and [Dy_2Ni] are presented here for example. For their X-ray crystal structures, magnetization curves with jumps, and other details, see the references.

Figure 1a shows the frequency vs. magnetic field diagram for [Dy_2Cu] together with the EPR spectra superposed. The resonance field was proportional to the frequency, as expected from the Zeeman effect. The g value was 2.07 from the slope, being compatible with the Cu signal. Extrapolation gives a critical field of 1.36 T. It is identical to the position of a 2-μ_B jump due to the Cu spin-flip in the magnetization curves. Therefore, [Dy_2Cu] has an energy-level crossing from the ground ferrimagnetic state to a ferromagnetic one at 1.36 T. By treating the Dy moments as Ising spins with $|J^z| = 15/2$, an exchange coupling model can be built involving a unique parameter (Fig. 2). We determined $J_{Dy\text{-}Cu}/k_B$ to be –0.126 K.

Figure 1b shows the result on [Dy_2Ni]. We found a few $g \approx 2$ lines with zero-field splitting and "forbidden" $g \approx 4$ lines. In sharp contrast to the [Dy_2Cu] case, the resonance fields are shifted by a negative bias field, suggesting the presence of ferromagnetic coupling. The data were analyzed using three parameters (J, D, and E), to give $J_{Dy\text{-}Ni}/k_B$ = +0.031 K. The level-crossing fields in the Zeeman diagram completely correspond to the magnetization jump positions.

Very recently the EPR and magnetic study on [$(Dy_2Cu_2)_n$] has been published [3]. In spite of an apparent complex situation (three independent exchange pathways, two Dy-Cu and one Cu-Cu, are present), our concept totally holds for this system. We successfully determined two $J_{Dy\text{-}Cu}$'s.

The HF-EPR technique is very useful for evaluation of the exchange coupling in such compounds. We could not directly observe Dy signals, but we clarified the environment of Cu and Ni ions as the exchange bias field from adjacent Dy ions. In our systematic research on 4f-3d magnets, determination of exchange couplings of isomorphous derivatives is of great interest. Studies on [Ln_2Cu], [Ln_2Ni], and [$(Ln_2Cu_2)_n$] involving Ln = Gd, Tb, Ho, Er etc. in place of Dy are now in progress.

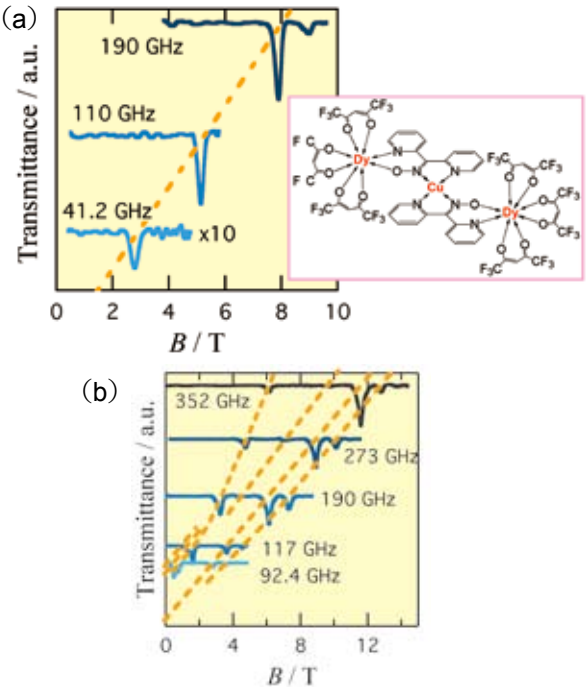

Fig.1. Selected EPR spectra measured at 4.2 K as a function of frequency for (a) [Dy_2Cu] and (b) [Dy_2Ni]. The spectra are offset in a linear scale of the frequency. Dotted lines are drawn for a guide to the eye. Structural formula of [Dy_2Cu] is also shown in (a).

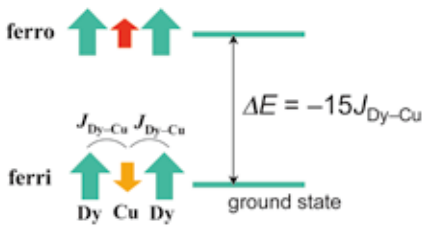

Fig.2. Energy diagram at zero-field for [Dy_2Cu]. Spin structures are drawn with arrows.

References

[1] F. Mori, T. Nyui, T. Ishida, T. Nogami, K.-Y. Choi, and H. Nojiri, J. Am. Chem. Soc., **128**, 1440 (2006).

[2] S. Ueki, T. Ishida, T. Nogami, K.-Y. Choi, and H. Nojiri, Chem. Phys. Lett., **440**, 263 (2007).

[3] A. Okazawa, T. Nogami, H. Nojiri, and T. Ishida, Chem. Mater., **20**, 3110 (2008).

Contact to
Takayuki Ishida (The Univ. of Electro-Communications)
e-mail: ishi@pc.uec.ac.jp
Hiroyuki Nojiri (Magnetism Division)
e-mail: nojiri@imr.tohoku.ac.jp

Pressure-induced Quantum Critical Phenomena in the *f* Electron Compound $CeTX_2$

Effect of pressure on the electronic states has been investigated in $CePtSi_2$ and $CeNiGe_2$ which crystallizes in an orthorhombic layered structure. The external pressure enhances the Kondo temperature T_K in both compounds. A pressure induced crossover exists in the electronic state around P_v~ 1.0 GPa in $CePtSi_2$.

$CeTX_2$ crystallizes in an orthorhombic $CeNiSi_2$-type layered structure (Cmcm), which is constructed from the deformed fragments of $CeGa_2Al_2$ and α-$ThSi_2$ structures [1]. The long *b*-axis induces the formation the flat Brillöuin zone, which might produce quasi-two dimensional electronic state and magnetic instability play an important role. In these compounds, competition between the Ruderman-Kittel-Kasuya-Yoshida (RKKY) interaction and Kondo effect was discussed by Doniach as a function of $|JN(0)|$, where J and $N(0)$ are the exchange interaction between the conduction electron and the localized 4*f* spin and the density of states at the Fermi level, respectively. The external pressure is one of the control parameters to tune the value J, which leads a long range magnetically ordered state, or results in a screening of the 4*f* moment by conduction electrons. In the present work, we describe the effect of pressure on the electronic states of $CePtSi_2$ and $CeNiGe_2$.

$CePtSi_2$ has the large electronic specific heat coefficient about γ= 600mJ/molK^2 and the antiferromagnetic order near T_N ~1.5 K. Fig. 1 shows the temperature dependence of the magnetic contribution of $CePtSi_2$ to the electrical resistivity ρ due to 4f electrons, ρ_{mag}, which is estimated by using the relation, ρ_{mag} = ρ($CePtSi_2$) - ρ($LaPtSi_2$). ρ($LaPtSi_2$) is assumed to indicate only the phonon contribution and to be independent of pressure. ρ_{mag} increases with decreasing temperature until it shows maximum (T_2) around 28 K at ambient pressure. Below T_2, a small shoulder (T_1) is observed in the ρ_{mag} at pressure below 0.4 GPa. T_1 and T_2 are shown by arrows in the inset of Fig. 1.

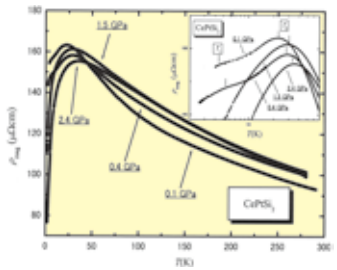

Fig.1. Temperature dependence of the ρ_{mag} of $CePtSi_2$ at high pressure.

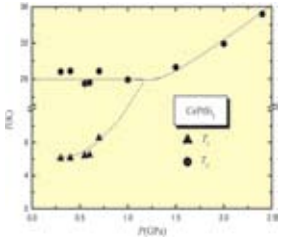

Fig.2. Pressure dependence of T_1 and T_2 of $CePtSi_2$.

Fig. 2 shows T_1 and T_2 as a function of pressure. T_2 is almost constant below 1.0 GPa, but T_1 increases with applying pressure and merges into T_2 around P_v~ 1.0 GPa, where the Kondo temperature T_K is close to T_K^h, a modified Kondo temperature due to the crystal electric field [2]. Similar behavior is found in $CeCu_2Si_2$, in which a quantum critical behavior is observed and the superconducting temperature T_{sc}(P) is enhanced around P_v~ 4.5 GPa [3].

Figure 3 shows the AC magnetic susceptibilities along the easy *c*-axis of $CeNiGe_2$ which orders magnetically at T_{N1}~ 4.0 K and undergoes a spin structure rearrengement at T_{N2}~ 3.0 K at ambient pressure. Here T_{N1} and T_{N2} are defined as the temperature where $d\chi_c/dT$ shows a kink while T_{max} is estimated as that where $d\chi_c/dT$ = 0 [4]. At ambient pressure, $d\chi_c/dT$ shows sharp anomalies at T_{N1} and T_{N2}, while T_{N1} is almost equal to T_{max} (= 4.0 K). As the pressure increases, some uncertainty as to the value of T_{max} arises because the magnitude of $d\chi_c/dT$ is suppressed and becomes zero in a wide temperature region. On the other hand, T_{N1} is suppressed by applying pressure but tends to saturate above 1.0 GPa. This behavior is contrary to the case of $CeAl_2$, $CeRh_2Si_2$, etc., in which the antiferromagnetic ordering temperature decreases as the pressure increases and quantum critical behavior is observed at the pressure near T_N ~0 K. T_{max} is almost the same as T_{N1} up to 0.68 GPa, indicating that T_{max} is related not only to the Kondo effect but also to the antiferromagnetic ordering. However, above 1 GPa, T_{max} increases with pressure and a rate of $\partial T_{max}/\partial P$ tends to be enhanced by applying pressure. Assuming that T_{max} indicates T_K in the pressure region, T_{max} is proportional to exp(1/$|JN(0)|$); the increase in T_{max} indicates the enhancement of $|JN(0)|$. In other words, the electronic state becomes unstable as pressure increases.

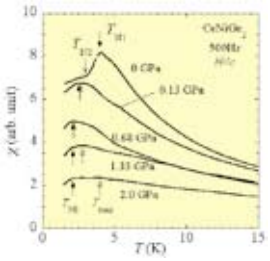

Fig.3 AC magnetic susceptibility of $CeNiGe_2$ under pressure.

In summary, it is found that T_K increases with pressure in both compounds. In $CePtSi_2$, a pressure induced crossover exists in the electronic state around P_v~ 1.0 GPa. In $CeNiGe_2$, on the other hand, further measurements above 2.0 GPa are in progress in order to determine a quantum critical behavior.

References

[1] M. Ohashi, G. Oomi, K. Ishida, T. Komatsubara, I. Satoh, *J. Alloys and Compounds* **408-412**, 84 (2006).

[2] H Miyagawa, Y Fuchizaki, M Ohashi, G. Oomi, I. Satoh, T. Komatsubara, *High Pressure Research* **26**, 503 (2006).

[3] A. T. Holmes, D. Jaccard, K. Miyake, *Physical Review B* **69**, 024508 (2004).

[4] M. Ohashi, G. Oomi, I. Satoh, *Journal of the physical society of Japan* **76**, 114712 1-3 (2007).

Contact to

Masashi Ohashi (Faculty of Environmental Design, Kanazawa University)

e-mail: ohashi@t.kanazawa-u.ac.jp

Isamu Satoh (Laboratory of α-Ray Emitters)

e-mail: satoh@imr.tohoku.ac.jp

Development of Co-Cr-Mo Alloys Containing Interstitial Elements with High Strength and High Ductility for Biomedical

Metallic biomaterials have been widely used for orthopedics and dental applications. Among various biomaterials, Co-Cr-Mo alloys are especially applied for load- and wear-bearing implants. The higher reliability of the implants is strongly required from the point of mechanical properties as well as biocompatibility recently.

Conventional cast and wrought Co-Cr-Mo alloys contain Ni to improve their castability and workability. However, Ni has been reported as one of the most common contact allergens. The cast alloys (ASTM F-75) show low ductility and the Co-based dental casting alloys occasionally fracture during small plastic deformation caused by the adjustment. Although Ni-free Co-Cr-Mo alloys have developed to avoid the allergic problem, the alloys still show the limited ductility owing to the shrinkage porosity and interdendritic segregation, which mainly consists of the σ phase. In addition, Ni-free Co-Cr-Mo alloys contains a large amount of ε martensite (hcp) in the γ (fcc) matrix, thereby restricting the deformation of the alloys [1,2]. Therefore, the suppression of the σ phase formation and the stabilization of the γ phase at room temperature are the key to enhance the mechanical properties of the alloy [3].

We focus boron and nitrogen as additives to the Co-Cr-Mo alloys, which are the interstitial elements and show no toxicity, to stabilize the γ phase (fcc). A large amount of stacking fault and ε martensite form along (111) plane in the Co-29Cr-6Mo alloy. Figure 1 shows TEM micrographs of B- and N- added Co-29Cr-6Mo alloy. ε martensite disappears and the γ phase is confirmed with low fault density in the Co-29Cr-6Mo alloy. In addition, the σ phase precipitation was confirmed to be suppressed by OM observation.

Figure 2 shows nominal stress-strain curves of various Co-Cr-Mo alloys. By the addition of B, elongation is improved although the yield strength is almost the same as Co-29Cr-6Mo. When N and B added to Co-29Cr-6Mo, both yield strength and elongations are clearly improved compared to Co-29Cr-6Mo. Therefore, it is confirmed that the addition of boron and nitrogen is very effective for the improvement of mechanical properties of Co-29Cr-6Mo alloys.

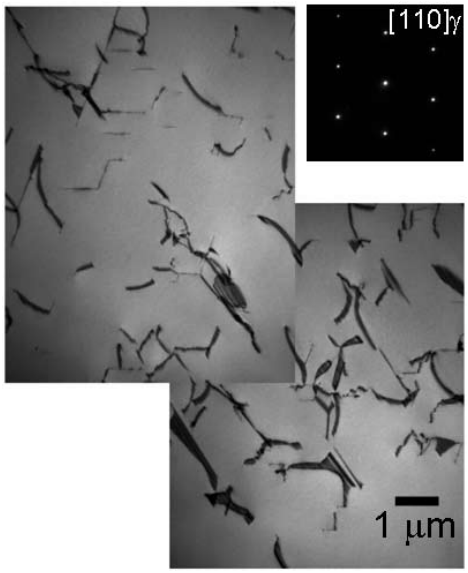

Fig. 1 TEM micrograph of B- and N- added Co-29Cr-6Mo alloy.

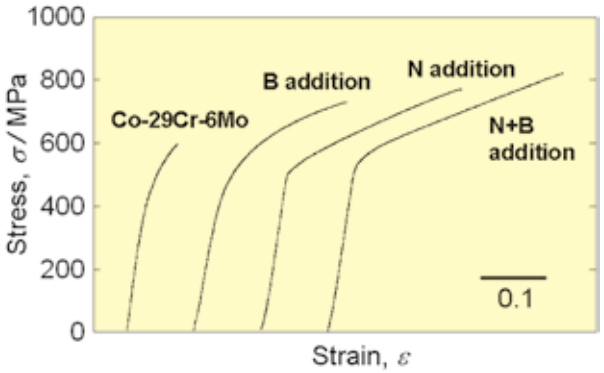

Fig. 2 Stress-strain curves of B- and /or N-added Co-Cr-Mo alloys.

Contact to
Naoyuki Nomura (Institute of Biomaterials and Bioengineering, Tokyo Medical and Dental University)
e-mail: nnomura.met@tmd.ac.jp
Akihiko Chiba (Deformation Processing Devision)
e-mail: a.chiba@imr.tohoku.ac.jp

References

[1] S-H. Lee, E. Takahashi, N. Nomura and A. Chiba, Mater. Trans. 46, 1790 (2005).
[2] S-H. Lee, T. Uchikanezaki, N. Nomura, M. Nakamura and A. Chiba, Mater. Trans. **48**, 1084 (2007).
[3] S-H. Lee, N. Nomura and A. Chiba, Mater. Trans. **49**, 260 (2008).

Neutron Damage Resistant SiC/SiC Composites by NITE Method

Based on the JMTR, JOYO, HFIR and other reactor irradiation and simulation radiation damage studies, neutron damage tolerant SiC/SiC composites have been designed and successfully fabricated by NITE method. They provide excellent mechanical properties, thermal and chemical stability, as well as gas tightness. Also model components for nuclear reactors were made and their excellent performance was confirmed.

SiC has a long history as one of the most attractive candidates for nuclear energy systems and many R & D has been carried out together with strong push by the invention of PCS-type SiC fibers by late Professor S. Yajima. Throughout the Japan-US collaborative activities on Fusion Materials, SiC and SiC/SiC R & D was extensively carried out and many insights about material behavior under neutron bombardment and reactor environments had been reported. Figure 1 is an example showing the excellent radiation damage resistance under neutron bombardment, where SiC/SiC made by CVI method kept its strength over 10dpa at elevated temperatures. Based on these neutron radiation effect results and simulation radiation effect study results, R & D direction of radiation damage tolerant SiC/SiC composites design and fabrication has been defined. The R & D direction is to fabricate (1) high crystallinity, (2) high purity, (3) near stoichiometry and (4) near full density in SiC fiber and SiC matrix together with the sound C or C/SiC interphase. At the same time, an innovative fabrication method, patented under the name of NITE (Nano Infiltration and Transient Eutectic Phase) method, has been developed for realizing the R & D direction by inexpensive process. This technology was transferred to a venture business from Kyoto University for establishing strong industrial basis to provide sufficient amount for the real utilization.

One of the important properties of NITE-SiC/SiC is the excellent gas tightness which indicates, for the first time, the potentiality to be applied for gas reactors and gas cooled blanket system for fusion reactors. More than 6 orders of magnitude improvement in He permeability has been confirmed, as shown in Figure 2, and the stability of this tightness even under the loading larger than proportional limit strength of SiC/SiC has been also published.

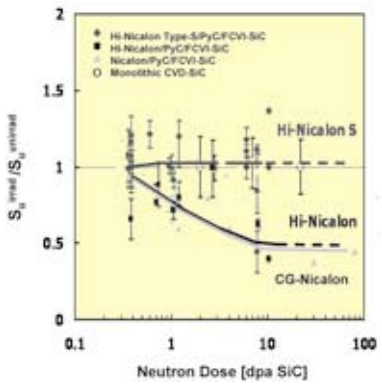

Fig. 1 Neutron damage effect on ultimate strength of SiC materials.

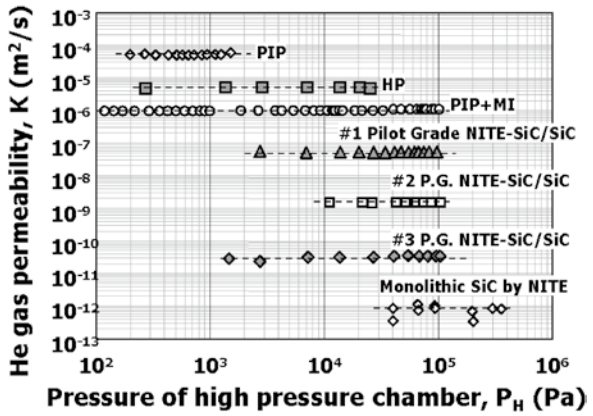

Fig. 2 He gas permeability of SiC materials.

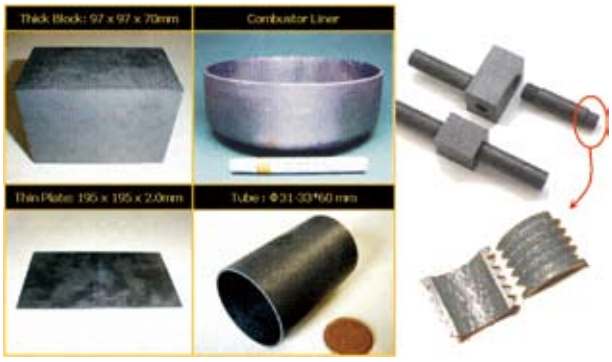

Fig. 3 Shape flexibility of NITE SiC/SiC.

Some of the typical SiC/SiC model components to be applied to Generation IV nuclear reactors and fusion reactors are shown in Figure 3, where thin tube for fuel pin application and its excellent machinability and excellent joint strength are indicated.

Porous SiC/SiC for TRISO fuel compartment for lateral flow gas cooling reactor core and full dense SiC/SiC for size model of intermediate heat exchanger (IHX) for many energy conversion systems have been also introduced. The effort starting from IMR-Oarai is one of the strong bases of the nuclear material community of Japan.

References

[1] Y. Katoh, T. Nozawa, L.L. Snead, T. Hinoki, A. Kohyama, Fusion Engineering and Design **81**, 937 (2006).
[2] K. Ozawa, T, Nozawa, Y. Katoh, T. Hinoki and A. Kohyama, J. Nucl. Mater., **367-370**, 713 (2007).
[3]J.S. Park, A. KohyamaT. Hinoki and K. Shimoda, J. Nucl. Mater., **367-370**, 719 (2007).

Contact to
Akira Kohyama (IAE, Kyoto University)
e-mail: kohyama@iae.kyoto-u.ac.jp
Minoru Narui (International Research Center for Nuclear Materials Science)
e-mail: narui@imr.tohoku.ac.jp

Anomalous Behavior at the Superconducting Upper Critical Field in Transuranium Superconductor $NpPd_5Al_2$

Magnetic behavior near the superconducting upper critical field H_{c2} of $NpPd_5Al_2$ has been studied at low temperature and high magnetic field. The strong XY-type magnetic anisotropy in the normal state suddenly disappears below H_{c2}. This result demonstrates that the superconductivity in $NpPd_5Al_2$ is carried by electrons having large magnetic moments with 5f character.

$NpPd_5Al_2$ is the first neptunium-based heavy fermion superconductor [1].This compound shows superconductivity at a fairly high superconducting transition temperature 5 K with typical heavy fermion behavior characterized by the large electronic specific heat in the normal state. It is also surprising that the isostructural compounds with the same structure have never been reported either in rare earth or actinide systems. Immediately after this discovery, scientists explored the An-Pd-Al phase again and revealed the existence of several actinide and rare earth $AnPd_5Al_2$ compounds like UPd_5Al_2 (An : rare earth or actinide elements) [2].

Compared to ordinary superconductors, the electrons in heavy fermion superconductors, in general, have the larger effective mass and the larger magnetic moment, both arising from the hybridization with the magnetic f-electrons. In the spin-singlet superconducting state, the large magnetic moment disappears by forming a Cooper pair with up- and down-spin electrons. Therefore, heavy fermion superconductivity is generally broken by magnetic field to gain Zeeman energy of unpaired quasiparticles. In $NpPd_5Al_2$, particularly, this occurs as a first-order phase transition [1].

In $NpPd_5Al_2$, the magnetic moments in the normal state have the XY-type anisotropy, namely, they tend to lie in the tetragonal basal plane and cannot be oriented along the [001] direction. It is therefore interesting to detect the change in the magnetic anisotropy through superconducting transition. Fig 1 shows the magnetic torque with the magnetic field applied around the [001] direction. In the normal state above the upper critical field H_{c2}, large magnetic torque is observed, which is attributed to the XY-type anisotropy. The present torque diminishes quickly with decreasing magnetic field through H_{c2}. Below H_{c2} there is no sizable torque detected, indicating quite isotropic magnetic behavior in the superconducting state. The magnetic field where the torque anomaly occurs exactly follows the H_{c2} determined from the resistivity, as shown in Fig. 2. Combining with the previous magnetization measurement [1], it is concluded that the large magnetic moment existing in the normal state disappears in the superconducting state. This result strongly suggests that the superconductivity in $NpPd_5Al_2$ is realized by the electrons with extremely large anisotropic magnetic moment.

This work was performed in collaboration with Osaka university.

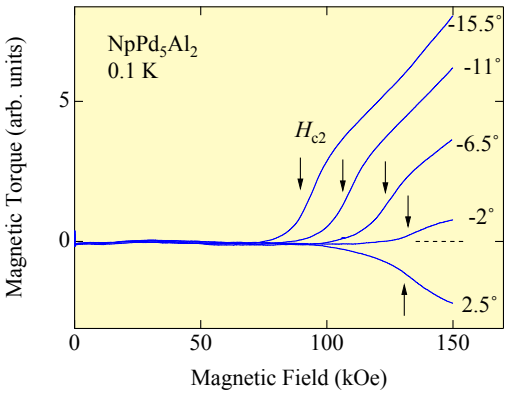

Fig. 1 Magnetic torque measured under magnetic field around [001] direction in $NpPd_5Al_2$. Arrows show the uppercritical field H_{c2}

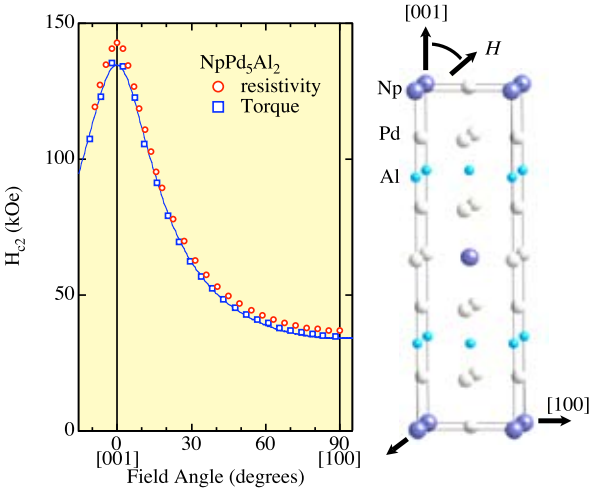

Fig. 2 Left: Angular dependence of the torque anomaly is compared to that of H_{c2} determined from resistivity measurements. Right: Crystal structure of $NpPd_5Al_2$.

References

[1] D. Aoki, Y. Haga, T.D. Matsuda, N. Tateiwa, S. Ikeda, Y. Homma, H. Sakai, Y. Shiokawa, E. Yamamoto, A. Nakamura, R. Settai and Y. Onuki, J. Phys. Soc. Jpn. **76** 063701 (2007).

[2] Y. Haga, D. Aoki, Y. Homma, S. Ikeda, T.D. Matsuda, E. Yamamoto, H. Sakai, N. Tateiwa, N.D. Dung, A. Nakamura, Y. Shiokawa and Y. Onuki, J. Alloys. Compds. (2008) in press.

Contact to
Yoshinori Haga (Advanced Science Research Center, JAEA)
e-mail: haga.yoshinori@jaea.go.jp
Yoshiya Homma (Radiochemistry of Metals Division)
e-mail: yhomma@imr.tohoku.ac.jp

Viscous Flow Behaviours of $Zr_{55}Cu_{30}Al_{10}Ni_5$ Bulk Metallic Glasses over the Entire Temperature Range

Viscous flow behaviors of $Zr_{55}Cu_{30}Al_{10}Ni_5$ bulk metallic glasses over the entire temperature range containing supercooled liquid region and the equilibrium liquid region has been examined. Viscosity has been measured by using a penetration viscometer under various heating rates in the supercooled liquid region and a containerless electrostatic levitation method in the equilibrium liquid region.

$Zr_{55}Cu_{30}Al_{10}Ni_5$ bulk metallic glasses (BMGs) have especially attached great interest due to their excellent properties such as very high glass forming ability that the alloys enable the formation of centimeter-sized cylindrical BMG samples and their excellent mechanical properties [1]. It has also been reported recently that a centrifugal casting method from the equilibrium liquid state of the BMGs is effective on fine precision molding [2]. In order to clarify the bulk glass forming process and also the fine precision molding process from the liquid state, the most important factor is the temperature dependence of the viscosity over the entire temperature range. We have reported the highly reliable viscosity of the $Zr_{55}Cu_{30}Al_{10}Ni_5$ supercooled liquids [3-5]. In the present study, temperature dependence of the viscosity of the $Zr_{55}Cu_{30}Al_{10}Ni_5$ BMGs has been examined over the entire temperature range containing supercooled liquid by a penetration viscometer and the equilibrium liquid regions by a .containerless electrostatic levitation method in high vacuum atmosphere [6].

Figure 1 shows the viscosity (η) of the $Zr_{55}Cu_{30}Al_{10}Ni_5$ supercooled liquids as a function of temperature at various heating rates of 20, 200 and 400 °C/min. In each heating condition, viscosity was measured under various applied loads of 0.049, 0.098, 0.196 and 0.294 N on the cylindrical indentation probe with a diameter of 1.0 mm. As shown in this figure, viscosity was quite independent of these applied loads under the various heating conditions. However, when the sample was slowly heated at the rate of 20 °C/min, viscosity exhibited relatively high values that may be mainly due to the skin effects of oxides on the sample surface. With increasing the heating rate to 200 °C/min, viscosity (η) largely decreased and the ln η decreased linearly with increasing the temperature up to about 470 °C and then increased with increasing the temperature for their crystallization. At the heating rate of 400 °C/min, viscosity was also exhibited relatively high values at a low temperature region between 400 and 450 °C. This may be due to the non-equilibrium liquid state under the high-speed heating condition. In the temperature region between 450 and 490 °C, viscosity fitted precisely to the linear relationship measured under the heating rate of 200 °C/min indicating the equilibrium viscosity may be measured in this temperature region. **Figure 2** shows the viscosity of the $Zr_{55}Cu_{30}Al_{10}Ni_5$ equilibrium liquid as a function of temperature that was obtained by the conteinerless electrostatic levitation method. The equilibrium viscosity exhibit very low values that are about $1x10^{10}$ times lower than that of the supercooled liquids. **Figure 3** shows a fragility plot of the viscosity of the $Zr_{55}Cu_{30}Al_{10}Ni_5$ alloys over the entire temperature range in comparison with some metallic and nonmetallic glass forming liquids. In this case, normalized Tg = 692 K (419 °C) was obtained by a Vogel-Fulcher-Tammann (VFT) relationship. As clearly shown in this figure, the $Zr_{55}Cu_{30}Al_{10}Ni_5$ alloy behaves closer to the strong glasses than the fragile glasses.

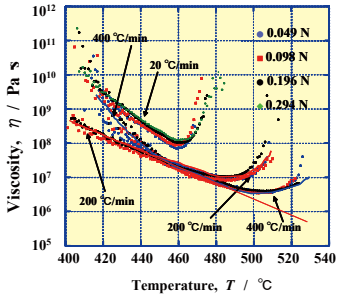

Fig. 1 Viscosity (h) of the $Zr_{55}Cu_{30}Al_{10}Ni_5$ supercooled liquids as a function of temperature at various heating rates of 20, 200 and 400°C/min.

References

[1] Y. Yokoyama, E. Mund, A. Inoue and L. Schlts, Mater. Trans. **48**, 3190 (2007).
[2] Y. Furuya, KINKEN Research Highlights 55 (2007).
[3] T. Yamasaki, S. Maeda, Y. Yokoyama, D. Okai, T. Fukami, H. M. Kimura and A. Inoue: Mater. Trans. **46**, 2746 (2005).
[4] T. Yamasaki, S. Maeda, Y. Yokoyama, D. Okai, T. Fukami, H. M. Kimura and A. Inoue, J. Intermetallics, **14**, 1102 (2006).
[5] T. Yamasaki, S. Maeda, T. Fukami, Y. Yokoyama,. H. M. Kimura and A. Inoue: Mater. Trans. **48**, 1834 (2007).
[6] T. Ishikawa and P. F. Paradis, Proc. of the 20th Space Utilization Symposium, **20**, 263 (2004).

Contact to
Tohru Yamasaki (Department of Materials Science and Chemistry, University of Hyogo)
e-mail: yamasaki@eng.u-hyogo.ac.jp
Yoshihiko Yokoyama (Advanced Research Center for Metallic Glasses)
e-mail: yy@imr.tohoku.ac.jp

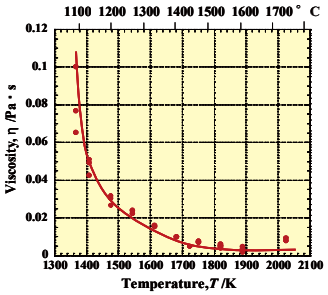

Fig. 2 Viscosity of the $Zr_{55}Cu_{30}Al_{10}Ni_5$ equilibrium liquids as a function of temperature measured be the containerless electrostatic levitation method.

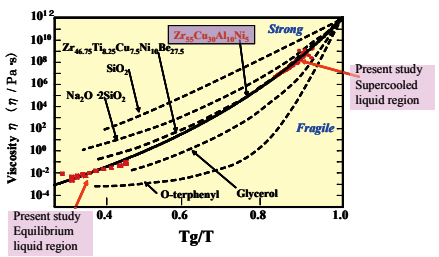

Fig. 3 Fragility plot of viscosity of the Zr-Cu-Al-Ni BMGs.

Elucidation of Magnetization Mechanism in Nd-Fe-B Thin Films by in-field Magnetic Force Microscopy

This article describes our recent results on Nd-Fe-B "hard magnetic" thin films. The samples were prepared onto single crystal MgO substrates using an UHV-compatible dc-sputtering system. A detailed magnetization behavior was observed by a magnetic force microscope (MFM) specially equipped with electro-magnet, which enables us to measure in-field magnetic domain structure.

Since a discovery of Nd-Fe-B permanent magnet [1], it has been widely and practically used as magnetomotive force for applications such as motors, actuators and sensors, because of its large magnetocrystalline anisotropy and high maximum energy products. From the recent environmental and energy issues, the consumption of Nd-Fe-B sintered magnets has been increased by the expansion of hybrid vehicles' (HVs) market. However, especially for HVs, in order to enhance the coercivity *Hc* at high temperature environments, the addition of heavy rare earth elements such as Tb and Dy to the Nd-Fe-B sintered magnets is essential. Recently, another problem of the amount of material resources has been occurred and it urges us to reduce the amount of these elements. In addition, the value of coercivity of Nd-Fe-B commercial magnets is still far from the theoretical prediction of $Nd_2Fe_{14}B$ alloy [2]. In this study, in order to compensate the gap between the experimental and theoretical value of coercivity, in other word, to elucidate the mechanism of the coercivity of Nd-Fe-B magnets, we have investigated the magnetic domain structure of the Nd-Fe-B thin films by magnetic force microscope specially equipped with electro-magnet [3].

All the samples were prepared using an UHV-compatible dc-sputtering system (base pressure < 1×10^{-8} Pa). A Cr seed layer of 1 nm and a Mo buffer layer of 20 nm were firstly deposited onto single-crystal MgO(110) substrates at room temperature. The nominal thickness of Nd-Fe-B layer *t* was 30 nm. The films were heated at 625 °C during the deposition of Nd-Fe-B layer. The magnetic properties were measured in the applied magnetic field perpendicular to the film plane by using a superconducting quantum interference device (SQUID) magnetometer in the field up to 55 kOe (for some cases, 70 kOe). The structural analysis was performed by an x-ray diffraction with Cu-Kα radiation.

Atomic force microscope (AFM) and MFM images of Nd-Fe-B thin film are shown in Fig. 1. Bright and dark contrast in MFM image represent an upward and downward magnetization direction, respectively. Magnetic fields during this measurement were applied from 0 to 6 kOe and 6kOe to -6kOe. A remarkable maze-like domain pattern was observed at virgin state of the film as shown in Fig. 1(b). With increasing an applied field, the region of dark stripe was gradually diminished (Fig.1 (b) to (d)). However, the stripes began to appear again after removing the applied field (Fig.1 (e)). It is noted that this stripe region is also observed at sintered magnet and this region is thought to be a "weak" hard magnetic region in the Nd-Fe-B thin film. The reduction of this "weak" region is thought to plays an important role to elucidate the magnetization mechanism.

References

[1] M. Sagawa, N. Togawa, H. Yamamoto, and Y. Matsuura, J. Appl. Phys., **55**, 2083 (1984).
[2] H. Kronmüler, Phys. Stat. Sol., **144**, 385 (1987).
[3] H. Ishioka, T. Sato, H. Kato, H. Fujino, and T. Shima, Digest book of Intermag2008, pp.230 (2008).

Contact to
Toshiyuki Shima (Faculty of Engng., Tohoku Gakuin University)
e-mail: shima@tjcc.tohoku-gakuin.ac.jp
Koki Takanashi (Magnetic Materials Division)
e-mail: koki@imr.tohoku.ac.jp

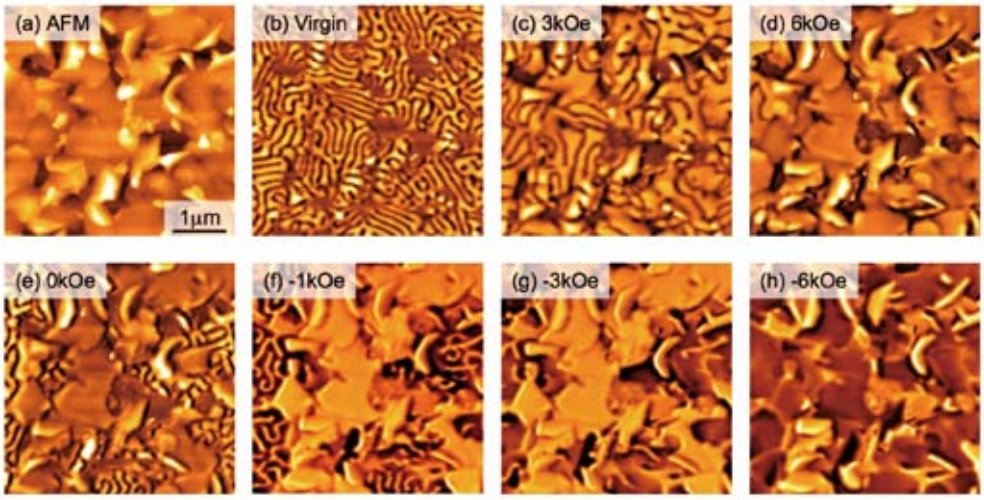

Fig. 1. Magnetic force microscope images for Nd-Fe-B thin films. The film thickness was 30 nm. In-field magnetic fields were applied during the magnetic domain observation. (a) Surface morphology (AFM image), MFM image of (b) virgin state, MFM images measured at H_{ex}= (c) 3kOe, (d) 6kOe, (e) 0kOe, (f) -1kOe, (g) -3kOe and (h) -6kOe. Bright and dark contrast in MFM image represent an upward and downward magnetization direction, respectively.

Immobilization of Poly(ethylene glycol) to Metal Surfaces with Electrodeposition

To bifunctionalize the surface of metals, poly(ethylene glycol), PEG, molecules are immobilized to titanium, cobalt-chromium-molybdenum alloy and 316L type stainless steel with electrodeposition. PEG molecules strongly and efficiently immobilized to titanium surface with electrodeposition, compared than that with immersion. In addition, concentration of active hydroxyl groups on surface oxides on metals influences the immobilization amounts of PEG. PEG-immobilized surface inhibited the adsorption of protein on titanium.

Recently, biofunctions are required for metals for biomedical use. For example, stents are placed at stenotic blood vessels for dilatation, and blood compatibility or prevention of adhesion of platelet is necessary. In guide wires and guiding cathetels, sliding lubrication in blood vessel is important when those are inserted into there. In addition, if metals were used for a sensing device, the control of cell adhesion is necessary. For these purposes, the fundamental property is inhibition of protein adsorption. Poly(ethylene glycol), PEG, is a biofuctional molecule on which adsorption of proteins is inhibited. Therefore, immobilization of PEG to metal surface is an important event to bio-functionalize the metal surface. No successful one-stage technique for the immobilization of PEG to base metals has ever been developed. In this study, PEG modified both terminals or one terminal with amine bases was immobilized onto titanium surface using electrodeposition. PEG modified at both terminals or one terminal with amine bases was immobilized onto titanium surface.

The bonding manner of PEG to titanium surface is significant to design PEG-immobilized materials, while characterization techniques for the determination of immobilization manner of PEG are a little. PEG terminated at both terminals or one terminal with amine bases was immobilized onto titanium surface with electrodeposition and immersion. The electrodepsition was carried out with -5V for 300 s. Immobilization manner of PEG was characterized using X-ray photoelectron spectroscopy (XPS) with angle-resolved technique and glow discharge optical emission spectroscopy (GD-OES). As a result, not only electrodeposition but also immersion led to the immobilization of PEG onto titanium surface. However, more terminated amines combined with titanium oxide as an ionic NH-O by electrodeposition, while more amines randomly existed as NH_3^+ in the PEG molecule by immersion. Moreover, the difference of amine termination led to different bonding manner, U-shape in PEG terminated both terminals and brush in PEG terminated one terminal. Characterization with XPS and GD-OES is useful to determine immobilization mode of PEG to solid surface [1,2].

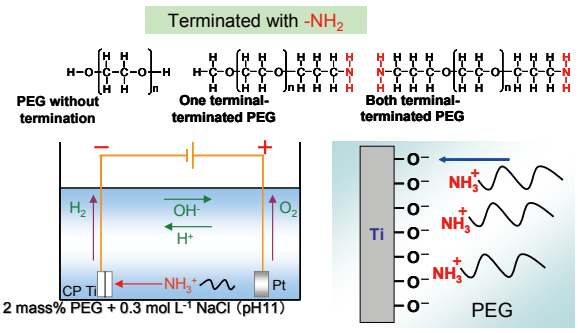

Fig. 1 PEG molecules were terminated with amine bases at one terminal or both terminals. Amine bases dissociate and are positively charged in aqueous solution and electrically attracted to titanium surface with cathodic charge, and eventually PEG molecules are immobilized.

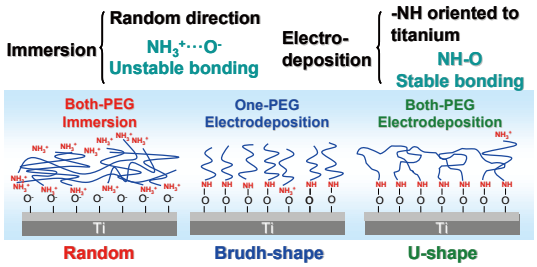

Fig. 2 Schematic model of iimobilized manners of PEG to titanium surface with immersion and electrodeposition. In the first layer of immobilized PEG formed by electrodeposition, more terminated amines exist at the interface between PEG layer and titanium oxide and combine with titanium oxide as N-HO bond ionic bond formed between NH_3^+ and OH^- while more amines randomly exist as NH_3^+ in PEG layer formed by immersion. In the both-terminated PEG, the PEG immobilized as a U-shape because both terminals combine with the titanium surface; in the one-terminated PEG, the PEG was immobilized as a brush because only one terminal combines with the surface. Over second layers, nitrogen atoms mainly exist as NH3+, while nitrogen locates a deeper site of PEG layer.

The concentrations of hydroxyl groups located inside and on the surface oxide films of a commercially pure titanium, cp-Ti, a type 316L austenitic stainless steel, SS, and a cobalt-chromium-molybdenum alloy, Co-Cr-Mo, were evaluated using X-ray photoelectron spectroscopy, XPS, and a zinc-complex substitution technique. As a result, the concentrations of the hydroxyl groups detected by the zinc-complex substitution technique, defined as active hydroxyl groups, were much larger than those detected by other conventional techniques. The concentration of the active hydroxyl groups on Co-Cr-Mo was significantly larger than those on cp-Ti and SS. Poly(ethylene glycol), PEG, is a biofunctional molecule that inhibits the adsorption of proteins. The immobilization of PEG to metal surfaces by electrodeposition or immersion is an important technique to biofunctionalize the metals. The amounts of the PEG layer immobilized on the metals were governed by the concentrations of the active hydroxyl groups on each surface oxide in the case of electrodeposition; it was governed by the relative permittivity of the surface oxide in the case of immersion. The estimation of active hydroxyl groups on the surface oxide film with the zinc-complex substitution technique is useful for the elucidation of reactions between metal substrates and immobilized molecules [3].

PEG-immobilized surface inhibited the adsorption of proteins, therefore, this electrodeposition technique is useful and universally biofinctionalize metal surfaces.

References

[1] Y. Tanaka, H. Doi, Y. Iwasaki, S. Hiromoto, T. Yoneyama, K. Asami, H. Imai and T. Hanawa, Mater. Sci. Eng. **C27**, 206 (2007).
[2] Y. Tanaka, H. Doi, E. Kobayashi, T. Yoneyama and T. Hanawa, Mater. Trans., **48**, 287 (2007).
[3] Y. Tanaka, H. Saito, Y. Tsutsumi, H. Doi, H. Imai and T. Hanawa, Mater. Trans., **49**, 805 (2008).

Contact to
Takao Hanawa (Institute of Biomaterials and Bioengineering, Tokyo Medical and Dental University)
e-mail: hanawa.met@tmd.ac.jp
Hisamichi Kimura (Advanced Research Center of Metallic Glasses)
e-mail: hisami@imr.tohoku.ac.jp

Transport Measurements of a Heavy Fermion Compound URu_2Si_2 under High Magnetic Field

Much attention has been attracted in the order parameter of elusive "hidden order" state in a heavy fermion compound URu_2Si_2. We have investigated the transport properties under high magnetic fields at low temperatures using an ultraclean single crystal of URu_2Si_2. The results suggest the band dependent nature of the hidden order gap.

URu_2Si_2 is a well known heavy fermion compound which has elusive "hidden order" (HO) state. The HO state realized below T_h = 17.5 K with a large entropy change. However, neutron scattering experiments reported a tiny ordered moment of 0.02 μ_B/U. Despite many experimental and theoretical efforts in the last two decades, the order parameter of the HO state is still unclarified.

We measured the transport properties in the HO state at high magnetic fields up to 27 T and low temperatures down to 0.5 K using an ultraclean single crystal of URu_2Si_2. Field dependence of the transverse magnetoresistivity ρ and Hall coefficient R_H (= $\rho_{xy}/\mu_0 H$), where ρ_{xy} is the Hall resistivity, are shown in Fig. 1 (a). Superconductivity sets in below the upper critical field $\mu_0 H_{c2}$ = 2.5 T. Above H_{c2}, the magnetoresistivity increases with increasing the field, has a plateau-like behavior between 18 to 22 T. The Hall coefficient has a sharp dip at $\mu_0 H^*$ = 22 T which is *lower* than the reported critical field (= 35 T) of the HO state. It is indicative of a phase transition *inside* the HO state. Above the plateau-like structure, ρ increases without saturation up to 27 T, reaches 1000 μΩ·cm which is 2000 times larger than that of zero field extrapolation. This huge magnetoresistivity comes from the cleanness of the sample and the compensation of electrons and holes. *H-T* phase diagram for *H* // [001] is shown in Fig. 1 (b). *H** (*T*) decreases with increasing the temperature as shown in red circles. We also observed clear oscillation in ρ and R_H due to the Shubnikov-de Haas (SdH) effect at high fields above around 20 T. Three fundamental branches, δ, α and β were observed. Figure 2 shows the angular dependence of the SdH frequency *F*. *F* (= $\hbar c S_F/2\pi e$) is proportional to the extremal (maximal or minimal) cross-sectional area of the Fermi surface S_F. Branches α, which is corresponding to a spherical Fermi surface, and β are in good agreement with the previous de Haas-van Alphen (dHvA) experiments. However, δ branch, which is clearly shows an elliptical Fermi surface, has not been reported in the dHvA experiment while it has relatively light cyclotron effective mass m_c = 2.7 m_0 for *H* // [001]. Branch δ begins to appear above around 20 T which is close to the phase transition.

From these results, we conclude that the HO gap on the newly-found elliptical Fermi surface is suppressed at high fields(HO I phase) while it is opened at low fields(HO II phase) (see Fig. 1 (b)). In analogy with the recently proposed multiband nature of the superconducting gap in this system[1], the present results suggest the *band dependent nature* of the HO gap in URu_2Si_2.

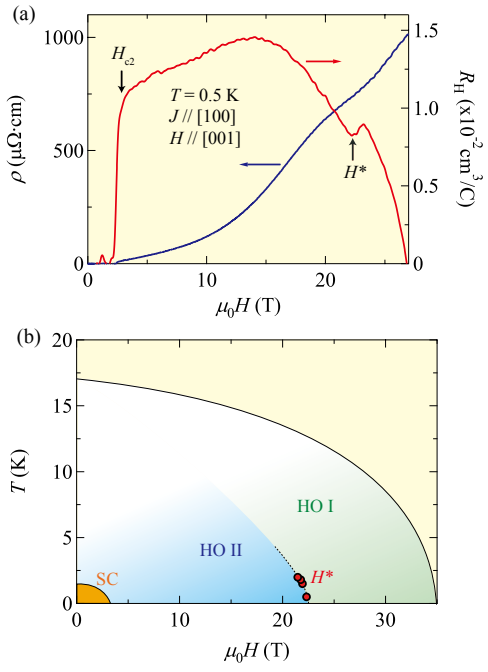

Fig. 1. (a) Field dependence of the Hall coefficient and transverse magnetoresistivity for *H* // [001] at *T* = 0.5 K. (b) *H-T* phase diagram for *H* // [001].

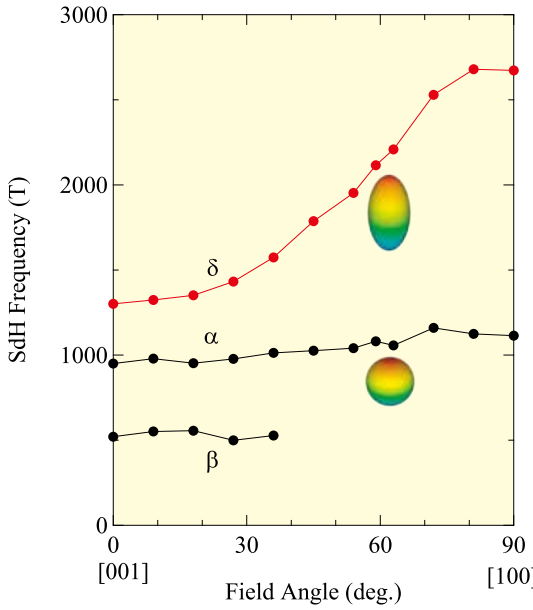

Fig. 2. Angular dependence of the SdH frequencies for branch δ, α and β, with schematic Fermi surfaces.

Reference

[1] Y. Kasahara, T. Iwasawa, H. Shishido, T. Shibauchi, K. Behnia, Y. Haga, T. D. Matsuda, Y. Onuki, M. Sigrist and Y. Matsuda, Phys. Rev. Lett. **99** 116402 (2007).

Contact to
Hiroaki Shishido (Department of Physics, Kyoto University)
e-mail: shishido@scphys.kyoto-u.ac.jp
Takahiko Sasaki (Low Temperature Physics Division)
e-mail: takahiko@imr.tohoku.ac.jp

Characterization of Current Transport Properties in High T_c Superconducting $RE_1Ba_2Cu_3O_{7-\delta}$ Coated Conductors Targeting High Field Magnet Applications

We have succeeded to describe nonlinear current transport properties in $RE_1Ba_2Cu_3O_{7-\delta}$ coated conductors as a function of temperature and magnetic field including very high fields more than 30 T. This allows us to design a high field superconducting magnet taking into account detailed operation conditions inside the magnet.

$RE_1Ba_2Cu_3O_{7-\delta}$ (RE=Rare earth elements; RE-123) coated conductor is one of the most promising superconducting materials especially for high field magnets because of its superior in-field critical currents and mechanical strength. Recently, remarkable progress has been achieved in the development of long length tapes in km-length scale with high current carrying capability. This demonstrates a big potential of those materials. However, fundamental current transport properties of those new wires were not yet fully understood for engineering applications.

Thermal stability of superconducting magnets can be improved drastically by using high critical temperature, T_c, superconducting (HTS) winding because 1) heat capacity increases several orders higher than the conventional ones at elevated operation temperature and 2) high T_c results in essential large temperature margin. This means that the design concept of superconducting magnet becomes quite different from the conventional one. Namely, we need to take into account dissipation inside the winding, which is originating from nonlinear electric field-v.s.-current density (*E-J*) characteristics in the superconducting strand. However, the current transport characteristics vary in a complicated manner depending on operation conditions such as temperature, magnetic field and applied field angle to the tape surface.

Based on a physical model describing percolative characteristics of current driven flux flow in a disordered medium, we have established a physical model which describes *E-J* characteristics in the HTS superconductors [1, 2]. Schematic diagram of the percolative flux flow is shown in Fig. 1 (a). Such percolative flux penetration has been confirmed indeed in coated conductors by the transport magnetic microscopy as shown in Fig. 1 (b) [2].

Within the framework of the percolation model, we formulate the nonlinear *E-J* characteristics analytically, and also predict the properties up to very high magnetic field [1, 3]. As an example, transport *E-J* characteristics in a Gd-123 coated conductor is shown in Fig. 2, where dots are measured results and lines are analytical expression. External field was applied 30 degree from tape surface as schematically shown

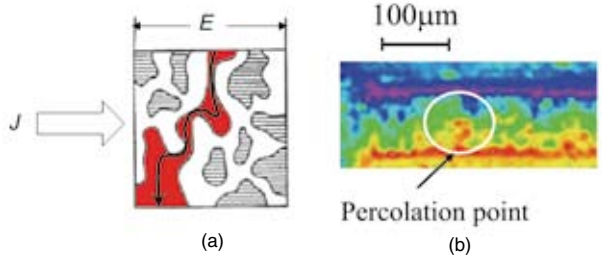

Fig. 1 (a) Schematic diagram of percolative flux flow and (b) visualized flux penetration into coated conductor by transport scanning SQUID microscopy.

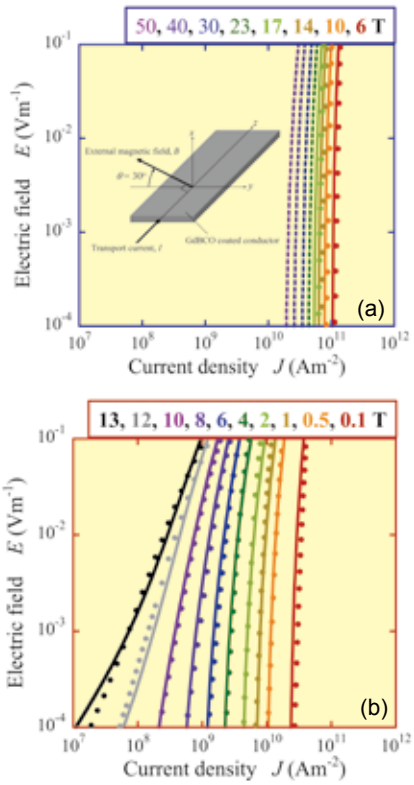

Fig. 2 Magnetic field dependent *E-J* characteristics in Gd-123 coated conductor (a) 4.2K and (b) 77K. Lines are analytical expression within the framework of the percolation model, whereas the dots are measurements.

in the inset of Fig. 2(a). Thickness of the superconducting layer in the tape is 1.2μm, therefore, it can be seen that more than several-100A of transport current can be carried by 1 cm wide tape even under very high external field more than 30 T. Properties at high temperature region is also well described by the same formulation as shown in Fig. 2(b).

References

[1] T. Kiss, M. Inoue, S. Egashira, T. Kuga, M. Ishimaru, M. Takeo, T. Matsushita, Y. Iijima, K. Kakimoto, T. Saitoh, S. Awaji, K. Watanabe, and Y. Shiohara, IEEE Trans. Appl. Supercond. **13**, 2607 (2003).

[2] T. Kiss, M. Inoue, T. Shoyama, S. Koyanagi, D. Mitsui, T. Nakamura, K. Imamura, A. Ibi, Y. Yamada, T. Kato, T. Hirayama, Y. Shiohara, IEEE Trans. Appl. Supercond. **17**, 3211 (2007).

[3] M. Inoue, T. Kiss, D. Mitsui, T. Nakamura, T. Fujiwara, S. Awaji, K. Watanabe, A. Ibi, S. Miyata, Y. Yamada and Y. Shiohara, IEEE Trans. Appl. Supercond. **17**, 3207 (2007).

Contact to
Takanobu Kiss (Research Institute of Superconductor Science and Systems, Kyushu University)
e-mail: kiss@sc.kyushu-u.ac.jp
Kazuo Watanabe (High Field Laboratory for Superconducting Materials)
e-mail: kwata@imr.tohoku.ac.jp

Development of a New Type of High-Temperature Structural Material based on Dual Multi-Phase Intermetallic Alloys

Dual multi-phase intermetallic alloys, which are composed of $Ni_3Al(L1_2)$ and Ni solid solution (A1) phases at high temperature and is additionally refined by a eutectoid reaction at low temperature, according to which the Al phase is decomposed into $Ni_3Al(L1_2)+Ni_3V(D0_{22})$, was developed. The alloys with such a novel microstructure showed extremely attractive high-temperature properties, promising for a new-type of high-temperature structural material.

A number of Ni-based superalloys currently in use are composed of a two-phase microstructure consisting of γ (Ni solid solution:A1 phase) and γ' (Ni_3Al:$L1_2$ phase). A1 phase is most densely packed structure when metal or alloy exists as a mono-component or a solid solution. On the other hand, $L1_2$ phase is categorized in geometrically close packed (GCP) structure. It has been believed that attractive properties of Ni-based superalloys are attributed to not only the presence of γ' ($L1_2$ phase) but also fine microstructure with coherency between Ni solid solution and γ'. Like the superalloys, the multi-phase intermetallic alloy composed of the GCP Ni_3X intermetallic phases is expected to have coherent interfaces and fine microstructure because of their closely related crystal structures.

The so-called dual multi-phase intermetallic alloy, which is composed of $Ni_3Al(L1_2)$ and Ni solid solution (A1) phases at high temperature annealing and is additionally refined by a eutectoid reaction at low temperature aging, according to which the Al phase is decomposed into the $Ni_3Al(L1_2)$+ $Ni_3V(D0_{22})$ phases, was recently developed, based on the pseudo-binary alloy system Ni_3Al-Ni_3V containing Ti and Nb [1,2]. It was shown that the dual multi-phase intermetallic alloys exhibit highly coherent interface structure between the constituent phases of $Ni_3Al(L1_2)$ and $Ni_3V(D0_{22})$ not only at the micron scale but also at the sub-micron scale as shown in Fig.1, and also display high microstructural and phase stability at high temperature [1,2].

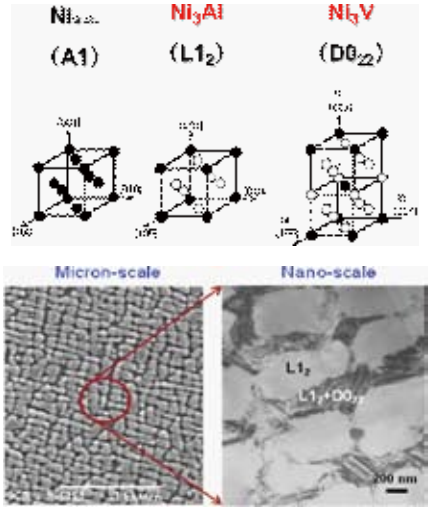

Fig. 1 Microstructure of dual multi-phase intermetallic alloy composed of geometrically close packed (GCP) structures $Ni_3Al(L1_2)$ and $Ni_3V(D0_{22})$.

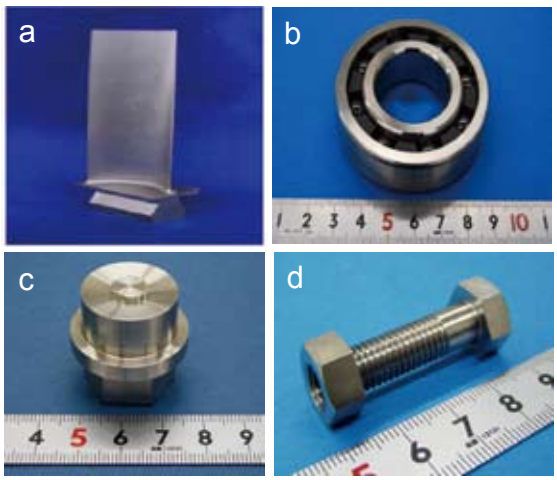

Fig. 2 Some products or parts fabricated by the dual multi-phase intermetallic alloy: (a) turbine blade for jet engine, (b) ball bearing, (c) friction stirring welding tool for high melting point materials, and (d) bolt and nut.

The dual multi-phase intermetallic alloys showed extremely high yield and tensile strengths with good temperature retention [3,4], and also superior oxidation resistance at high temperature and corrosion resistance in various liquids. Over a broad temperature range, high tensile elongation and fracture toughness were observed. The creep test conducted at high temperature showed the presence of high threshold stress, and also extremely low creep rate and long creep rupture time when compared with conventional Ni-based superalloys [3,4]. The obtained results are promising for the development of the dual multi-phase intermetallic alloy as a new-type of high-temperature structural material. Figure 2 indicates some products and parts actually fabricated by the dual multi-phase intermetallic alloys. In collaboration with industries not only in Kansai area but also in Keihin area, the development based on the dual multi-phase intermetallic alloys is currently conducted.

References

[1] Y. Nunomura, Y. Kaneno, H. Tsuda and T. Takasugi, Acta Materialia, **54**, 851 (2006).
[2] W. Soga, Y. Kaneno and T. Takasugi, Intermetallics **14**, 170 (2006).
[3] S. Shibuya, Y. Kaneno, M. Yoshida and T. Takasugi, Acta Materialia, **54**, 861 (2006).
[4] W. Soga, Y. Kaneno, M. Yoshida and T. Takasugi, Mater. Sci. Eng. A, **473**, 180 (2008).

Contact to
Takayuki Takasugi (Graduate School of Engineering, Osaka Prefecture University)
e-mail: takasugi@mtr.osakafu-u.ac.jp
Toyohiko Konno (Osaka Center for Industrial Materials Research)
e-mail: tjkonno@imr.tohoku.ac.jp

A Review Book "Nano-and Micromaterials" Published as a New Volume of Advances in Materials Research from Springer

As a comprehensive scientific report of collaborated researches performed by Yokohama National University (YNU) and Institute for Materials Research (IMR), Tohoku University, a new review book titled "Nano- and Micromaterials" (picture) was published in February 2008 from Springer-Verlag as the ninth volume of the Springer series, "Advanc es in Materials Research" [1].

A fruitful IMR Collaborated Research in Priority Area named "Nanotechnology Research by First-Principles Calculations" has continued for three years between Kaoru Ohno's group at YNU and Yoshiyuki Kawazoe's group at IMR. Also in YNU, an interdisciplinary research project named "Materials Science for Nano- and Micro-Scale Control: Creation of New Structures and Functions" (Leader: Kaoru Ohno, Subgroup Leaders: Masatoshi Tanaka and Jun Takeda) has continued at the same time period. This book edited by K. Ohno, M. Tanaka, and J. Takeda (YNU), and Y. Kawazoe (IMR) collects review articles on the recent progress in variety of subjects written by the members in both YNU and IMR under these research projects. The content of this book is as follows:

Chap. 1 "General Introduction" (K. Ohno, YNU) pp.1-17.
Chap. 2 "Nanometer-Scale Structure Formation on Solid Surfaces" (M. Tanaka, K. Shudo, S. Ohno, YNU) pp.19-95.
Chap. 3 "Ultrafast Laser Spectroscopy Applicable to Nano- and Micromaterials" (J. Takeda, YNU) pp.97-119.
Chap. 4 "Defects in Anatase Titanium Dioxide" (T. Sekiya and S. Kurita, YNU) pp.121-141.
Chap. 5 "Organic Radical 1,3,5-Trithia-2,4,6-Triazapentalenyl (TTTA) as Strong Correlations Electronic Systems: Experiment and Theory" (J. Takeda, Y. Noguchi, S. Ishii, and K. Ohno, YNU) pp.143-169.
Chap. 6 "Ab Initio **GW** Calculations Using an All-Electron Approach" (S. Ishii, K. Ohno, and Y. Kawazoe, IMR) pp.171-188.
Chap. 7 "First-principles Calculations Involving Two- Particle Excited States of Atoms and Molecules Using T-Matrix Theory" (Y. Noguchi, S. Ishii, and K. Ohno, YNU) pp.189-217.
Chap. 8 "Green's Function Formulation of Electronic Transport at Nanoscale" (A. A. Farajian, O. V. Pupysheva, B. I. Yakobson, and Y. Kawazoe, IMR) pp.219-241.
Chap. 9 "Self-Assembled Quantum Dot Structure Composed of III-V Compound Semiconductors" (K. Mukai, IMR) pp.243-262.
Chap. 10 "Potential-Tailored Quantum Wells for High-Performance Optical Modulators/Switches" (T. Arakawa and K. Tada, YNU) pp.263-274.
Chap. 11 Thermodynamic Properties of Materials Using Lattice-Gas Models with Renormalized Potentials (R. Sahara, H. Mizuseki, K. Ohno, and Y. Kawazoe, IMR) pp.275-290.
Chap. 12 Optically Driven Micromachines for Biochip Application (S. Maruo, YNU) pp.291-309.
Chap. 13 Study of Complex plasma (M. Shindo and O. Ishihara, IMR) pp.311-327.

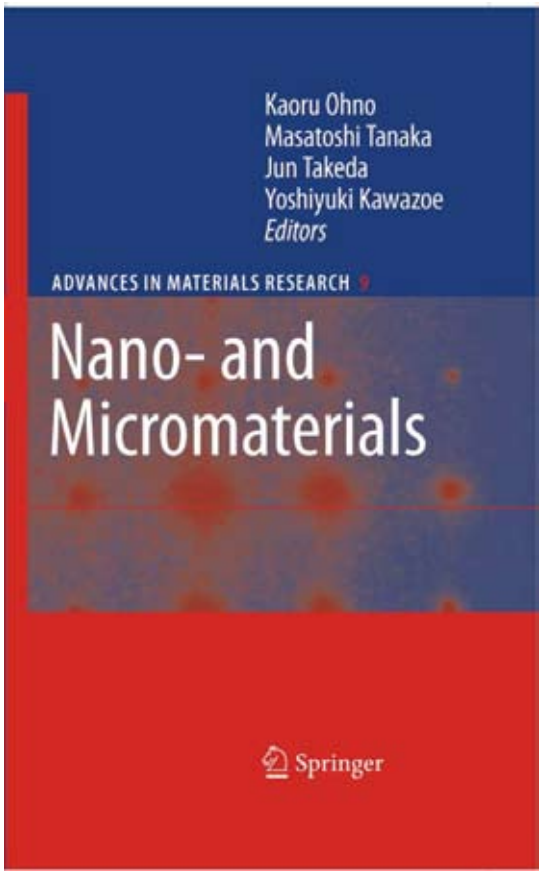

Reference

[1] K. Ohno, M. Tanaka, J. Takeda, and Y. Kawazoe, edited, "Nano- and Micromaterials", Springer Series on Advances in Materials Research, Vol. 9, Series Editors: Y. Kawazoe, M. Hasegawa, A. Inoue, N. Kobayashi,a nd T. Sakurai (Springer-Verlag, Berlin, Heidelberg, 2008) pp. 1-337

Contact to
Kaoru Ohno (Department of Physics, Graduate School of Engineering, Yokohama National University)
e-mail: ohno@ynu.ac.jp
Yoshiyuki Kawazoe (Materials Design by Computer simulation Division)
e-mail: kawazoe@imr.edu